

VARIABLE HEATING AND FLARING OF THREE REDBACK MILLISECOND PULSAR COMPANIONS

PATRICIA B. CHO, JULES P. HALPERN, AND SLAVKO BOGDANOV

Department of Astronomy, Columbia University, 550 West 120th Street, New York, NY 10027-6601, USA; patricia.cho@columbia.edu
Draft version September 5, 2018

ABSTRACT

We are monitoring established and putative redback millisecond pulsars (MSPs) in time-series photometry, repeatedly covering their 5–6 hr orbital light curves in r' or R . On timescales of months, PSR J1048+2339 and XMMU J083850.38–282756.8 exhibit similar variability of ≈ 0.3 mag on the heated side of the companion star. However, the heating light curve is rarely symmetric, suggesting that the intrabinary shock generated by the pulsar wind is skewed in addition to being variable, or that changing magnetic fields intrinsic to the companion channel the pulsar wind. In addition to this variable heating, there are long-lived flaring states that increase the brightness by an additional 0.5 mag, with variability on ≈ 10 minute timescales. These flares also appear to originate on the heated side of the companion, while the “night”-side brightness remains relatively stable. Somewhat less active, PSR J1628–3205 has an optical light curve that is dominated by tidal distortion (ellipsoidal modulation), although it too shows evidence of variable and asymmetric heating due to shifting magnetic fields or migrating star spots. These effects frustrate any effort to derive system parameters such as inclination angle and Roche-lobe filling factor from optical light curves of redback MSPs. We also report on two *Chandra* X-ray observations of PSR J1048+2339 that show strong orbital modulation, possibly due to beaming along the intrabinary shock, and a third observation that is dominated by flaring. The peak flare luminosity in the 0.3–8 keV band is $\approx 12\%$ of the pulsar’s spin-down power, which may require magnetic reconnection. None of these three systems has yet shown a transition back to an accreting state.

Keywords: gamma rays: stars — pulsars: individual (XMMU J083850.38–282756.8, PSR J1048+2339, PSR J1628–3205)

1. INTRODUCTION

The Large Area Telescope on the *Fermi Gamma-ray Space Telescope* is making a major contribution to the science of millisecond pulsars (MSPs). Of the 216 γ -ray pulsars detected to date, 99 are MSPs¹. The unique conditions under which MSPs are formed from their low-mass X-ray binary (LMXB) progenitors, and the continued episodic accretion that some of them display, provide new opportunities to explore interesting problems such as the nature of propeller accretion and the maximum mass of a neutron star.

MSPs are neutron stars with spin periods even faster than those of young pulsars. The recycling scenario is now widely understood to be the mechanism for their “spin-up”. An accretion disk fed by material stripped from a Roche lobe filling companion transfers angular momentum to the neutron star. In this way the neutron star spin periods are “recycled” into the millisecond regime (Alpar et al. 1982). Black widows (BWs) and redbacks comprise the subclass of MSPs whose binary orbits are $\lesssim 1$ day and whose radio pulses are often periodically eclipsed. An intrabinary shock driven by the relativistic pulsar wind produces a secondary wind of ablated plasma trailing off of the companion star (Phinney et al. 1988). While the cross-sectional area of the companion star alone would be insufficient to eclipse the signals for the durations observed, the companion’s plasma wind is extensive enough to disperse and absorb the radio pulsations as the neutron star reaches superior conjunction.

BW companion masses range from $\approx 0.01 - 0.05 M_{\odot}$ and redback companions range from $\approx 0.1 - 0.5 M_{\odot}$. The compact binary orbits often tidally distort their companion stars, which is evident as ellipsoidal orbital modulation. The optical light curves of many BW and redback systems also show heating on the side of the companion reaching in toward the inner Lagrange point (Romani & Shaw 2011; Kong et al. 2012; Breton et al. 2013; Gentile et al. 2014; Bogdanov et al. 2011, 2014a,b). This phenomenon, as well as orbitally modulated, power-law X-ray emission, lends further credence to the presence of an intrabinary shock. The amplitude of the modulation is proportional to the inclination of the binary system’s orbital plane, with the maximum possible modulation corresponding to an inclination angle of 90° .

There are over 60 BW and redback pulsars known,² almost equally divided between globular clusters and the Galactic field. Most of them were discovered in follow-ups of *Fermi* sources, which preferentially detect these subclasses of MSPs. In addition, there are several putative BWs or redbacks that are very likely counterparts of *Fermi* sources (see Li et al. 2018 for a list). The systems we investigate here are all *Fermi* sources: two previously confirmed redbacks exhibiting some evidence of heating, PSR J1628–3205 and PSR J1048+2339 (Li et al. 2014; Deneva et al. 2016), and one putative redback, XMMU J083850.38–282756.8 identified with 3FGL J0838.8–2829 (Halpern et al. 2017b). The goals of these observations are to characterize long-term vari-

¹ <https://confluence.slac.stanford.edu/display/GLAMCOG/Public+List+of+LAT-Detected+Gamma-Ray+Pulsars>

² <https://apatruno.wordpress.com/about/millisecond-pulsar-catalogue/>

Table 1
Log of Time-Series Photometry

| Telescope | Filter | Date (UT) | Time (UTC) | Phase (ϕ) ^a |
|--------------------------|-----------|-------------|-------------|-------------------------------|
| PSR J1048+2339 | | | | |
| 1.3 m | <i>R</i> | 2016 Jan 10 | 05:51–10:01 | 0.31–0.98 |
| 1.3 m | <i>R</i> | 2016 Jan 12 | 05:59–13:30 | 0.32–1.56 |
| 1.3 m | <i>V</i> | 2016 Jan 13 | 05:49–13:33 | 0.28–1.56 |
| 1.3 m | <i>R</i> | 2016 Mar 4 | 03:03–08:40 | 0.41–1.31 |
| 1.3 m | <i>R</i> | 2016 Mar 5 | 04:16–08:59 | 0.60–1.37 |
| 1.3 m | <i>R</i> | 2016 Mar 7 | 02:29–08:40 | 0.28–1.30 |
| 1.3 m | <i>R</i> | 2016 May 29 | 03:41–06:19 | 0.78–1.20 |
| 1.3 m | <i>R</i> | 2016 May 31 | 03:23–06:12 | 0.71–1.16 |
| 1.3 m | <i>R</i> | 2016 Jun 3 | 03:20–05:58 | 0.67–1.10 |
| 2.4 m | <i>r'</i> | 2016 Jun 7 | 03:29–05:48 | 0.67–1.04 |
| 1.3 m | <i>R</i> | 2016 Dec 24 | 07:35–13:18 | 0.70–1.64 |
| 1.3 m | <i>R</i> | 2017 Feb 27 | 02:35–07:03 | 0.34–1.07 |
| 1.3 m | <i>R</i> | 2017 Mar 24 | 03:06–10:05 | 0.22–1.34 |
| 1.3 m | <i>V</i> | 2017 Mar 25 | 02:43–09:09 | 0.15–1.20 |
| 1.3 m | <i>r'</i> | 2018 Jan 12 | 06:43–13:25 | 0.38–1.48 |
| 1.3 m | <i>r'</i> | 2018 Jan 14 | 06:57–13:29 | 0.41–1.48 |
| 1.3 m | <i>r'</i> | 2018 Feb 18 | 05:42–13:06 | –0.86–1.10 |
| 1.3 m | <i>r'</i> | 2018 Feb 22 | 07:43–13:05 | 0.21–1.10 |
| 1.3 m | <i>r'</i> | 2018 Apr 19 | 02:43–09:09 | –0.09–0.97 |
| 1.3 m | <i>r'</i> | 2018 Apr 20 | 02:41–08:51 | –0.10–0.99 |
| 1.3 m | <i>R</i> | 2018 Apr 21 | 02:34–09:00 | –0.13–0.93 |
| 1.3 m | <i>r'</i> | 2018 May 20 | 03:34–07:00 | 0.78–1.34 |
| 1.3 m | <i>r'</i> | 2018 May 21 | 03:15–06:03 | 0.72–1.18 |
| XMMU J083850.38–282756.8 | | | | |
| 2.4 m | <i>r'</i> | 2016 Dec 27 | 07:02–12:41 | 0.04–1.12 |
| 2.4 m | <i>r'</i> | 2017 Feb 25 | 02:57–08:20 | –0.05–0.98 |
| 1.3 m | <i>r'</i> | 2017 Nov 17 | 09:36–12:57 | 0.52–1.16 |
| 1.3 m | <i>r'</i> | 2017 Nov 19 | 09:41–13:00 | –0.13–0.50 |
| 1.3 m | <i>r'</i> | 2017 Dec 14 | 08:01–13:17 | 0.09–1.10 |
| 1.3 m | <i>r'</i> | 2017 Dec 16 | 07:38–12:54 | 0.33–1.34 |
| 1.3 m | <i>r'</i> | 2018 Jan 13 | 08:52–11:18 | 0.10–0.56 |
| 1.3 m | <i>r'</i> | 2018 Feb 23 | 03:06–08:21 | 0.11–1.11 |
| 1.3 m | <i>r'</i> | 2018 Mar 16 | 02:23–07:16 | –0.14–0.79 |
| PSR J1628–3205 | | | | |
| 2.4 m | <i>R</i> | 2014 May 26 | 05:58–09:36 | 0.88–1.60 |
| 2.4 m | <i>R</i> | 2014 May 27 | 06:04–09:37 | 0.70–1.40 |
| 2.4 m | <i>R</i> | 2014 May 28 | 05:34–09:28 | 0.41–1.18 |
| 2.4 m | <i>R</i> | 2017 May 29 | 05:12–09:59 | 0.72–1.66 |
| 2.4 m | <i>R</i> | 2018 May 20 | 05:37–10:38 | 0.15–1.14 |

^a Orbital phase zero corresponds to the ascending node of the pulsar.

ations in pulsar wind heating of the companions, and to search for flaring. In addition to these three variable objects, we have several observations of three more redbacks that show little if any change; these will be reported separately. Section 2 describes our observations and data reduction methodology. In Sections 3–5 we present new light curves and compare them with previous observations. Section 6 discusses the implications of the changes in the light curves, and we present our conclusions in Section 7.

2. OBSERVATIONS

We obtained new time-series photometry on 33 nights between 2016 Jan and 2018 May. All observations were performed using MDM Observatory’s 1.3 m McGraw-Hill Telescope or 2.4 m Hiltner Telescope on Kitt Peak. For observations on the 1.3 m, we used the thinned, backside-illuminated SiTe CCD “Templeton” which has a plate scale of $0''.509 \text{ pixel}^{-1}$. For observations on the 2.4 m, we used the Ohio State Multi-Object Spectrograph (OS-

MOS, Martini et al. 2011) in imaging mode. The OS-MOS plate scale is $0''.273 \text{ pixel}^{-1}$. Most images were taken in the *R* or *r'* filters. CCD readouts for observations done using the 2.4 m were binned to reduce dead-time, as this could be done without compromising the quality of the photometry. Exposure times were all 300 s except for data taken in the *V* filter for which exposure times were 360 s. Dead-time was 26 s for all exposures except for the binned 2.4 m images where dead-time was 13 s. A log of the observations is given in Table 1.

We used standard IRAF routines to reduce the images. We used *zerocombine* and *flatcombine* each in conjunction with *ccdproc* in the noao.imred.ccdred package to process the bias and twilight flat-field images. We used *ccdproc* to subtract the bias from and flatten the science images. We performed differential time-series photometry using *phot* in the noao.digiphot.daophot package. The parameters in *phot* were optimized based on the full width half maximum (FWHM) of the PSF for the pulsar companion and comparison stars. We also performed differential photometry on the comparison stars for each set of exposures against secondary comparisons to ensure they are not themselves variable. The same set of comparison and secondary comparison stars were also measured across different sets of exposures to confirm the absence of any long term variability. Absolute photometric calibration of comparison stars for PSR J1628–3205 was performed using a set of observations of Landolt (1992) standard stars taken on 2017 June 2. Magnitudes of comparison stars for PSR J1048+2339 and XMMU J083850.38–282756.8 were taken from SDSS and, where needed, converted to *V* and *R* using Lupton (2005) transformations³.

Previously published data from 2014 on PSR J1628–3205 (Li et al. 2014) were reextracted; differential photometry was conducted using the same set of comparison stars used previously and calibrated to the same secondary standards as the new data. There are some minor discrepancies between the light curves presented here and those from (Li et al. 2014), presumably due to slight differences in the parameters used to extract the photometry.

Figures in the following sections plot calibrated magnitude as a function of orbital phase for each set of exposures, where $\phi = 0$ corresponds to the ascending node of the pulsar. We first corrected each exposure to Barycentric Dynamical Time (TDB). To determine the orbital phase for the two radio pulsars, we calculated the number of orbital periods that had elapsed from the time of ascending node to the midpoint of the exposure using the radio pulsar ephemerides. For XMMU J083850.38–282756.8 we used the data themselves to fit a revised orbital ephemeris using the method of Halpern et al. (2017b), in which a fit to the minimum of the light curve was used to define the epoch assumed to be the inferior conjunction of the companion ($\phi = 0.25$). A few outlying points were deleted because they were affected by cosmic-ray contamination, and a few others that had very large errors were not used.

3. PSR J1048+2339

³ <http://classic.sdss.org/dr4/algorithms/sdssUBVRITransform.html>

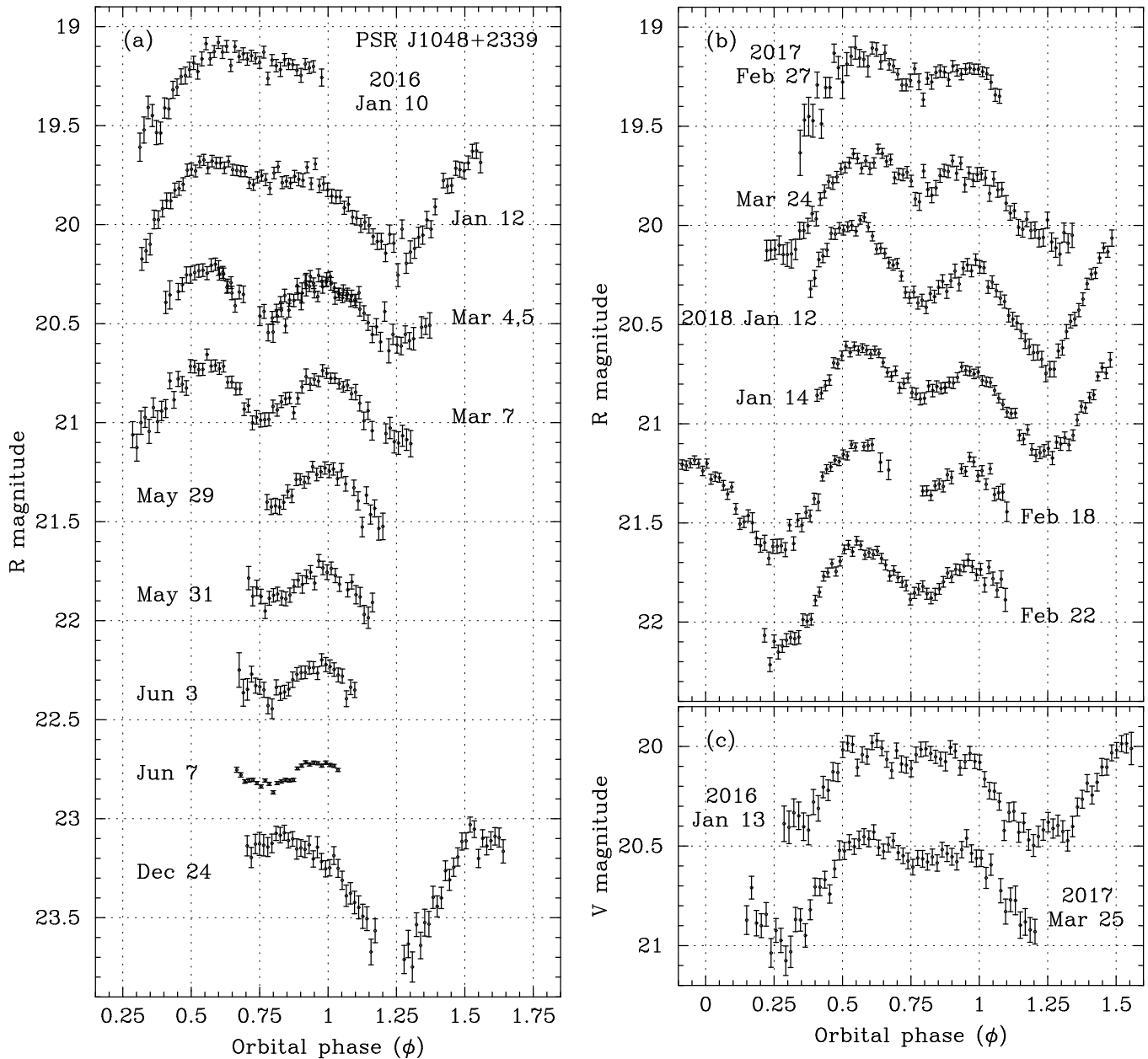


Figure 1. Optical light curves of PSR J1048+2339 as a function of orbital phase. A log of the observations is given in Table 1. In each panel data sets below the uppermost one are displaced downward by a multiple of 0.5 mag for clarity.

3.1. Optical Light Curves

Figures 1 and 2 show light curves of PSR J1048+2339 folded on the radio pulsar ephemeris of Deneva et al. (2016). Specifically, we use the (6.01 hr) orbital period and time of ascending node, but not the period derivative(s), which are not predictive on long timescales. Our earliest data from 2016 January (Figure 1a) resemble the mean light curve in the discovery paper (Deneva et al. 2016), which was extracted from the 2005–2013 Catalina Real-Time Transient Survey (CRTS). In particular, there is a minimum as expected at $\phi = 0.25$, the inferior conjunction of the secondary, and a downward sloping plateau from $0.5 < \phi < 1.0$ that is evidently due to pulsar heating of the companion, but not exactly symmetric about the expected $\phi = 0.75$. Such effects were pre-

viously noted and interpreted as asymmetric heating in other redback systems (Woudt et al. 2004; Li et al. 2014; Halpern et al. 2017b).

There subsequently appeared a significant change at $\phi = 0.75$, the expected phase of maximal heating. By 2016 March the brightness at this phase dipped by as much as 0.4 magnitudes below the maximum at $\phi = 0.5$, leaving two clearly defined peaks that are the signature of ellipsoidal modulation. In the absence of any heating, ellipsoidal modulation would be characterized by two equal maxima at $\phi = 0$ and $\phi = 0.5$, while the minimum at $\phi = 0.75$ would be deeper than that at $\phi = 0.25$ due to gravity darkening. While heating was still evident because the brightness at $\phi = 0.75$ remained higher than at $\phi = 0.25$, heating was no longer dominant over tidal

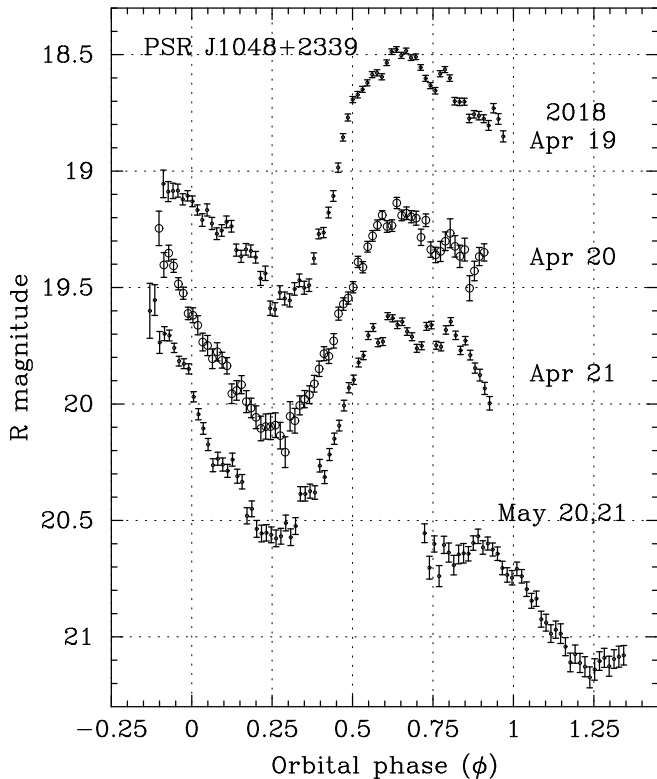


Figure 2. Optical light curves of PSR J1048+2339 in its flaring state in 2018 April, and having returned to the quiescent level in May. A log of the observations is given in Table 1. Each data set after April 19 is displaced downward by a multiple of 0.5 mag for clarity. The different symbols aid in the separation of closely spaced light curves.

distortion in shaping the light curve. Seasonal visibility restrictions then prevent us from getting complete orbital coverage, but by 2016 December 24 it appeared that heating had returned to its initial strength at $\phi = 0.75$.

Figure 1b shows additional light curves obtained in 2017 and 2018, which display a variety of levels of heating. These states are characterized by varying depths of the local minimum at $\phi = 0.75$, and also by significant changes in the relative heights of the two peaks at $\phi = 0.5$ and $\phi = 1.0$. While major changes appear on time scales of months, small variations can also take place in days, such as in the peak brightness between 2018 January 12 and 14.

Close examination reveals that the minimum expected at $\phi = 0.75$ doesn't always fall exactly at this phase, but after 2016 March is delayed by ≈ 0.05 . This shift is unlikely to be due to a drift in the orbital ephemeris because the phase of the primary minimum (viewing the dark side of the companion) remains consistent with $\phi = 0.25$ throughout. It may be the result of a number of different physical mechanisms. First, the skewed intrabinary shock that causes the sloping maxima and asymmetric peaks may also move the phase of minimum. Second, the companion may have a large starspot that occupies a position near the inner Lagrange point. Third, a shifting magnetic field intrinsic to the companion may channel the pulsar wind to a different location on its surface.

We obtained only two nights of data in the *V* filter for PSR J1048+2339, in 2016 and 2017. These two light curves closely resemble the *R*-band data at the

same epochs, and are reminiscent of the transitional MSP J1023+0038 in its radio pulsar state (Woudt et al. 2004; Thorstensen & Armstrong 2005).

In 2018 April we observed a new, flaring state for three consecutive nights (Figure 2). One month later, the light curve had returned to the quiescent level. The flaring state is characterized by up to an additional 0.5 mag brightening on the heated side of the star, which previously had $R \gtrsim 19.0$, but now reached up to $R = 18.5$. In addition, rapid variability on timescales of 10 minutes is evident. It is possible that faster variations could be detected with higher time resolution data. In addition, there may be rapid variability during some of quiescent periods in Figure 1, but this is less certain.

The existence of occasional flaring states was inferred in Deneva et al. (2016) from the couple of dozen observations out of the ≈ 400 from the CRTS that were up to a magnitude brighter than the average plateau. It appears that the location of the flares, as well as the more general long-term variability, are confined to side of the companion facing the pulsar, because the magnitude at $\phi = 0.25$, centered on the dark side, has remained relatively stable throughout our monitoring. We see that always $R \approx 19.6$ at $\phi = 0.25$, with a maximum range of ± 0.1 . Any systematic variation due to the calibration process is limited to ± 0.02 mag, so ± 0.1 mag is a conservative upper limit on the range of intrinsic stellar variability. Thus, the much larger change of up to 1 mag at other phases is not intrinsic to the companion star alone, but is related to and requires the influence of the pulsar.

3.2. X-ray Observations

We obtained three observations of PSR J1048+2339 with the *Chandra* Advanced Camera for Imaging and Spectroscopy (ACIS) S33 CCD, each spanning slightly more than one pulsar orbit. Details are listed in Table 2 and the light curves are shown in Figure 3. The first two observations have similar flux and a strongly modulated light curve with a minimum centered at $\phi = 0.25$, which is a common feature among redbacks. The third observation has a higher count rate and is dominated by flaring.

The shape of the first two light curves is sometimes interpreted as X-rays emitted by an intrabinary shock very close to the companion being partly occulted at inferior conjunction of the star (Bogdanov et al. 2011). However, such an effect would tend to produce a double-peaked light curve, whereas the data are statistically consistent with a broad, single peak.

Instead, beaming of synchrotron due to bulk relativistic motion along the limbs of the intrabinary shock may be the dominant effect on the light curve, as modelled by Romani & Sanchez (2016) and Wadiasingh et al. (2017). In this case, the nature of the light curve depends on the location and shape of the intrabinary shock, which in turn is determined by the relative momentum of the companion and pulsar winds. There is some evidence that companion wind may be the stronger one in PSR J1048+2339 as its radio pulsations are never detected during $0.02 < \phi < 0.49$ (Deneva et al. 2016), almost half the orbit, and are sporadically eclipsed at other phases as well. Since the companion wind is responsible for the

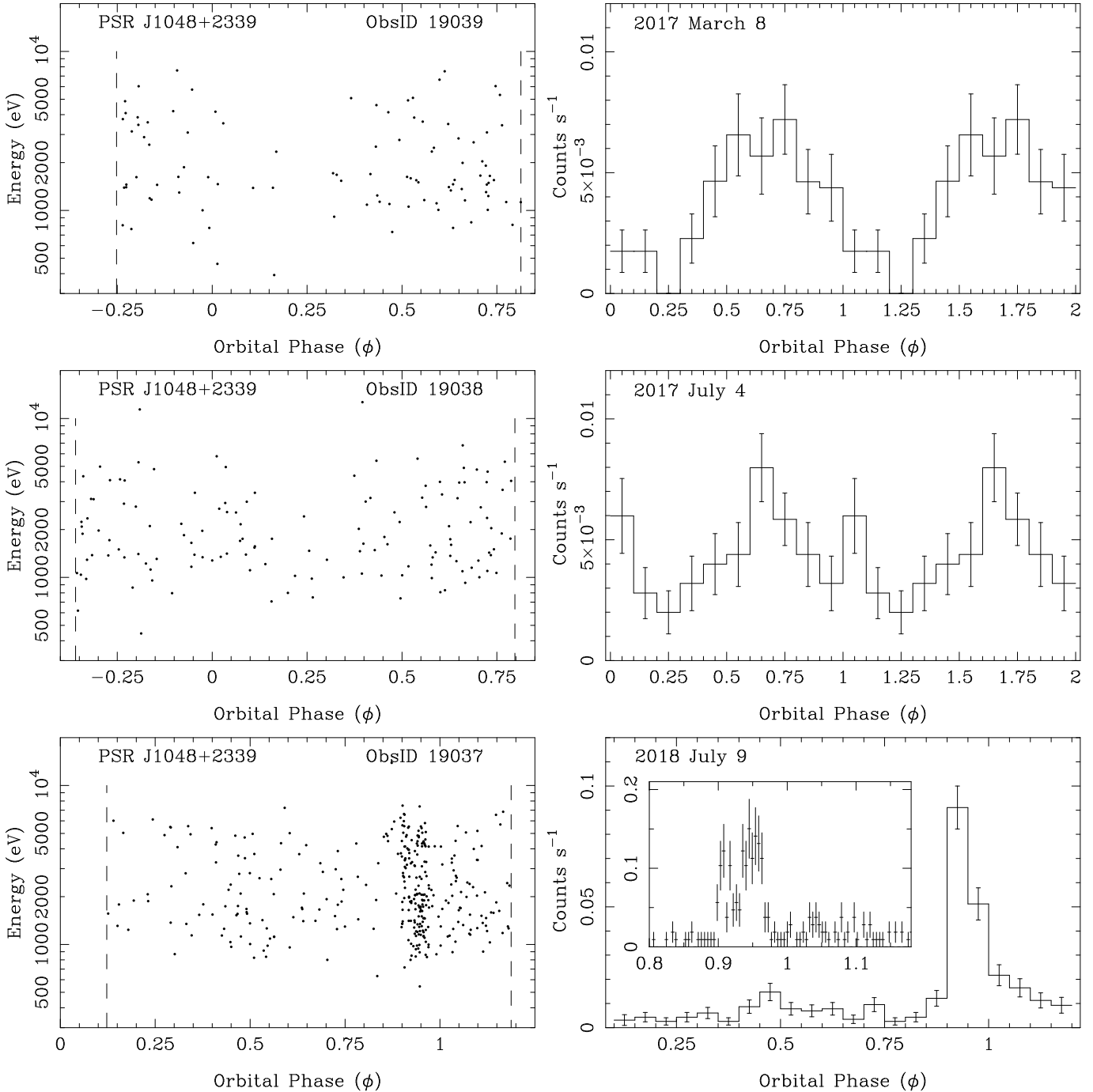


Figure 3. *Chandra* light curves of PSR J1048+2339 from three observations. The left-hand panels show the orbital phase and energy of each photon, with the vertical dashed lines marking the start and end of the observation. Each observation spans slightly more than one pulsar orbit. The right-hand panels are the binned light curves corrected for exposure time at each orbital phase. In the first two observations the binned light curve is repeated for clarity. The third observation is dominated by flares. The inset shows the main flare in 100 s bins.

radio absorption, this means that the intrabinary shock may be wrapped around the pulsar rather than around the companion, with the X-ray emission beamed toward the observer at $\phi = 0.75$. A broad, single X-ray peak could be seen at this phase if the bulk velocities along the shock are mildly relativistic, or the inclination angle of the orbit is not too large (Wadiasingh et al. 2017; Romani & Sanchez 2016).

Power-law spectral fits consistent with synchrotron emission are given in Table 2, where the N_{H} is either a

free parameter or fixed at the total Galactic value along the line of sight; the choice makes little difference. The count rates adjusted for effective exposure at each orbital phase are not significantly different for the first two (“quiescent”) observations. While the flux appears to have changed, this is mostly due to the additional time spent at brighter orbital phases in the second observation.

In order to estimate the X-ray luminosity we have to consider distance estimates based on the dispersion mea-

Table 2
Chandra X-ray Spectral Fits for PSR J1048+2339

| ObsID | Date (UT) | Exposure (s) | Counts | Rate ^a (s ⁻¹) | N_{H} (10 ²⁰ cm ⁻²) | Γ | F_X^{b} (0.3–8 keV) | χ^2/dof |
|--------------------------|------------------|--------------|--------|--------------------------------------|---|------------------------|------------------------------|---------------------|
| 19039 | 2017 March 8 | 22,551 | 98 | 0.0039(4) | 4_{-4}^{+69} | $1.56_{-0.56}^{+1.34}$ | $5.1_{-1.3}^{+6.5}$ | 3.02/3 |
| | | | | | 2.5 ^c | $1.56_{-0.50}^{+0.49}$ | $5.1_{-1.3}^{+1.5}$ | 3.02/4 |
| 19038 | 2017 July 5 | 24,729 | 136 | 0.0044(4) | 6_{-6}^{+43} | $1.54_{-0.41}^{+0.78}$ | $7.4_{-1.6}^{+3.1}$ | 2.11/6 |
| | | | | | 2.5 ^c | $1.46_{-0.36}^{+0.36}$ | $7.3_{-1.5}^{+1.6}$ | 2.14/7 |
| 19038+19039 | 2017 March, July | 47,280 | 234 | 0.0042(3) | < 20 | $1.47_{-0.29}^{+0.43}$ | $5.9_{-1.0}^{+1.1}$ | 9.42/12 |
| | | | | | 2.5 ^c | $1.51_{-0.30}^{+0.31}$ | $5.9_{-1.0}^{+1.0}$ | 9.63/13 |
| 19037 | 2018 July 9 | 22,753 | 344 | 0.0151(8) | < 17.5 | $1.23_{-0.19}^{+0.27}$ | $23.0_{-2.5}^{+2.6}$ | 19.27/19 |
| | | | | | 2.5 ^c | $1.26_{-0.19}^{+0.19}$ | $23.0_{-2.5}^{+2.6}$ | 19.49/20 |
| 19037 flare ^d | 2018 July 9 | 7,162 | 243 | 0.0339(22) | < 24.7 | $1.18_{-0.23}^{+0.38}$ | $51.9_{-6.9}^{+7.5}$ | 12.51/12 |
| | | | | | 2.5 ^c | $1.22_{-0.24}^{+0.23}$ | $52.0_{-6.8}^{+7.4}$ | 12.62/13 |

^a Phase-averaged count rate and uncertainty.

^b Unabsorbed 0.3–8 keV flux in units of 10^{-14} ergs cm⁻² s⁻¹.

^c N_{H} held fixed at the Galactic value from Kalberla et al. (2005).

^d Flare analysis includes all photons after $\phi = 0.85$ in Figure 3.

Table 3
 Photometric Orbital Ephemeris of XMMU J083850.38–282756.8

| Parameter | Value |
|---------------------------------------|--|
| R.A. (J2000) ^a | 08 ^h 38 ^m 50 ^s .416 |
| Decl. (J2000) ^a | –28°27′57″.03 |
| Time span (MJD) | 57071–58193 |
| Epoch T_0 (MJD TDB) ^b | 57781.2515(9) |
| Orbital period P_{orb} (day) | 0.2145229(6) |

^a Position from Pan-STARRS1 (Flewelling et al. 2016).

^b Epoch of ascending node of the putative pulsar, $\phi = 0$ in Figure 4.

sure ($DM=16.65$ pc cm⁻², Deneva et al. 2016). Distance is uncertain for MSPs at high Galactic latitude, like PSR J1628–3205, because it depends on the unknown scale height of the electron density distribution. The distance to PSR J1628–3205 from the NE2001 electron density model of Cordes & Lazio (2002) is 0.7 kpc. However, Deneva et al. (2016) calculated that the companion star would significantly underfill its Roche lobe at this distance, which is generally not the case for redbacks, and argues for a larger value. In fact, two revised models of the electron density distribution that incorporate a thick disk (Schnitzler 2012; Yao et al. 2017) both predict a distance of ≈ 2 kpc. Adopting this value, the 0.3–8 keV X-ray flux for the two combined quiescent observations in Table 2 corresponds to $L_x = 2.8 \times 10^{31}$ ($d/2$ kpc)² erg s⁻¹.

The third light curve is clearly dominated by flaring, with the main flare beginning at $\phi = 0.85$. The inset in Figure 3, which has 100 s bins, shows that the flare has structure on this timescale. The photon energies change over the flare; the first peak is harder than the second. Even before the main event there seems to be lower-level activity, with a small peak at $\phi = 0.5$ that is higher than the usual quiescent maximum at $\phi = 0.75$. We made two spectral fits, one for the entire observation, and another for the main flare from $\phi = 0.85$ to the end of the observation. Both fits have harder spectra than the quiescent state, as listed in Table 2. The flare has

$\Gamma \approx 1.2$ while the quiescent observations have $\Gamma \approx 1.5$, although these differ at only the 1σ level.

Note that the peak flare count rate of ≈ 0.14 s⁻¹ is 33 times higher than the mean of the quiescent observations. This implies that the peak 0.3–8 keV luminosity is $\approx 9.4 \times 10^{32}$ ($d/2$ kpc)² erg s⁻¹, which is $\approx 12\%$ of the pulsar’s spin-down power (Deneva et al. 2016). Here we have corrected the apparent spin-down power for the kinematic (Shklovskii 1970) effect using the Gaia measured proper motion of $(\mu_\alpha, \mu_\delta) = (-16.28 \pm 1.00, -11.70 \pm 1.27)$ mas yr⁻¹ (Gaia Collaboration et al. 2016a,b), resulting in $\dot{E} = [1.16 - 0.32(d/2 \text{ kpc})] \times 10^{34}$ erg s⁻¹.

4. XMMU J083850.38–282756.8

XMMU J083850.38–282756.8 is a putative redback identified with 3FGL J0838.8–2829. Its 5.15 hr orbital light curve, as noted by Halpern et al. (2017b), bears a strong resemblance to that of PSR J1048+2339. In Figure 4 we show two of the six light curves from the previous paper for comparison with new data obtained in 2017 November – 2018 March. It is evident that in 2016 until at least 2017 March, the star was in a flaring state very similar to that of PSR J1048+2339 in Figure 2, with rapid variability and brightness on the heated side that is ≈ 0.5 mag higher than it was in subsequent, quiescent periods. There may be also be rapid variability during some of quiescent episodes, particularly on 2017 December 14 and 16.

In the quiescent state of late 2017 – 2018 a slight dip appears around $\phi = 0.75$, indicating that ellipsoidal modulation may have a significant effect on the shape of the light curve. Similar to PSR J1048+2339, the minimum flux of XMMU J083850.38–282756.8 at $\phi = 0.25$ has remained comparatively constant, at $r' \approx 20.5 \pm 0.1$. However, this is a fainter star, sometimes difficult to measure accurately at minimum because of its southerly declination (high airmass) and a bright, neighboring star. Its calibration is also less accurate, with possible systematic variation of ± 0.035 mag. Nevertheless the apparent upper limit of ± 0.1 mag on the range of intrinsic stellar variability at $\phi = 0.25$ is much less than the observed range of ≈ 0.8 mag at the opposite phase of the orbit.

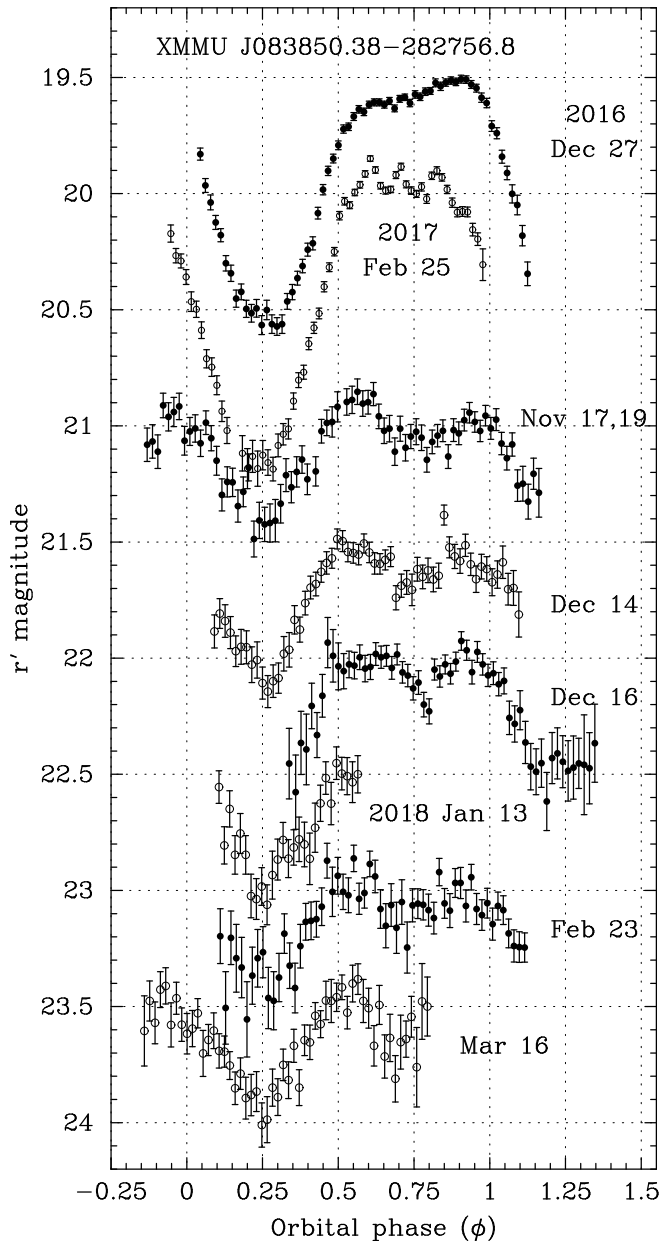


Figure 4. Optical light curves of XMMU J083850.38–282756.8 as a function of orbital phase according to the ephemeris in Table 3. Previously published observations from 2016 December and 2017 February are shown for comparison with new data from 2017 November – 2018 March. A log of all the observations is given in Table 1. Each data set after 2016 December 27 is displaced downward by a multiple of 0.5 mag for clarity. The different symbols aid in the separation of closely spaced light curves.

Thus, we conclude that variable heating and flaring is confined to the side of the companion facing the pulsar.

With the new data, we were also able to fit a refined orbital ephemeris using the method described in Halpern et al. (2017b), in which the epoch of minimum in the light curve is used as the fiducial phase $\phi = 0.25$. The longer baseline also enables us to extrapolate backward with a precise cycle count to an observation obtained on 2015 February 18 (Figure 7 of Halpern et al. 2017a). This is the earliest known light curve of the star, before its orbital period was apparent, but it contains a dip which provides another timing for phase 0.25. The

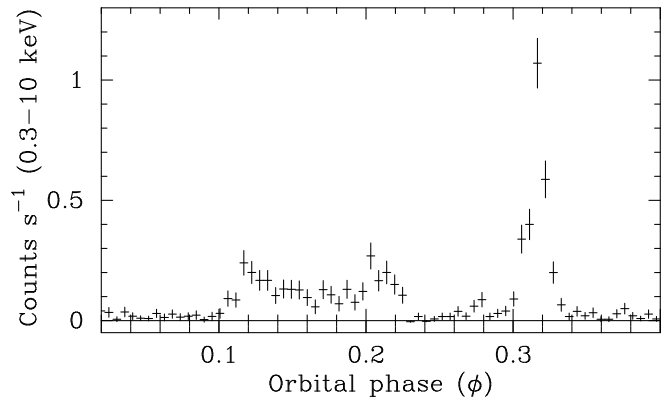


Figure 5. Background-subtracted *XMM-Newton* light curve of the 1.2 hr flaring episode of XMMU J083850.38–282756.8 on 2015 December 2 (ObsID 079080101), adapted from Halpern et al. (2017b). The bin size is 100 s. The revised orbital ephemeris of Table 3 was used.

resulting phase-connected ephemeris spans 3 years, and improves the precision of the previously published orbital period by an order of magnitude. In Table 3 we list the revised orbital parameters, as well as the position from Pan-STARRS1 (Flewelling et al. 2016), which differs by $0''.4$ from the position derived in Halpern et al. (2017b) based on USNO B1.0 astrometry.

Using the new ephemeris, which spans the epoch of the *XMM-Newton* observation of 2015 December 2 (ObsID 079018010), we are able to assign a precise orbital phase to the dramatic 1.2 hr long X-ray flare (Halpern et al. 2017b) seen in that light curve. Figure 5 shows the flaring segment with its three peaks spanning $0.10 < \phi < 0.34$. (An accompanying optical flare, observed with lower time resolution, is not reproduced here). Note that the phase has changed by 0.15 from the extrapolation of the former ephemeris that did not span the epoch of the X-ray observation. Interestingly, this event is almost centered on inferior conjunction of the secondary star, unlike all of the other flares reported here. Because of the complex temporal structure, it is not clear whether the quiescent level around $\phi = 0.25$ is an interval between spikes, or an eclipse by the secondary.

5. PSR J1628–3205

PSR J1628–3205 was first studied optically by Li et al. (2014) in 2014 May, where its 5.00 hr light curve appeared to be dominated by ellipsoidal modulation. We fold the data on an unpublished orbital ephemeris that spans 3 years from 2010 November to 2013 November, with $T_0 = 55514.86519315(12)$ MJD, $P_{\text{orb}} = 0.2081445829(9)$ d (S. Ransom 2014, private communication). As before, we use only the leading term because period derivatives, needed to fit slow wandering by tens of seconds in the time of ascending node (e.g., Deneva et al. 2016), are small and are not predictive outside the span of the ephemeris.

In Figure 6 we show the 2014 data with the best-fit (by eye) model of ellipsoidal modulation from that study, where only a lower limit on the inclination angle, $i > 55^\circ$, could be determined. The representative model shown has $i = 75^\circ$. Asymmetries in the data, deviating from the model, could only be explained by invoking off-center heating effects, starspots, or magnetic channeling of the pulsar wind. In 2017 May we obtained an additional light

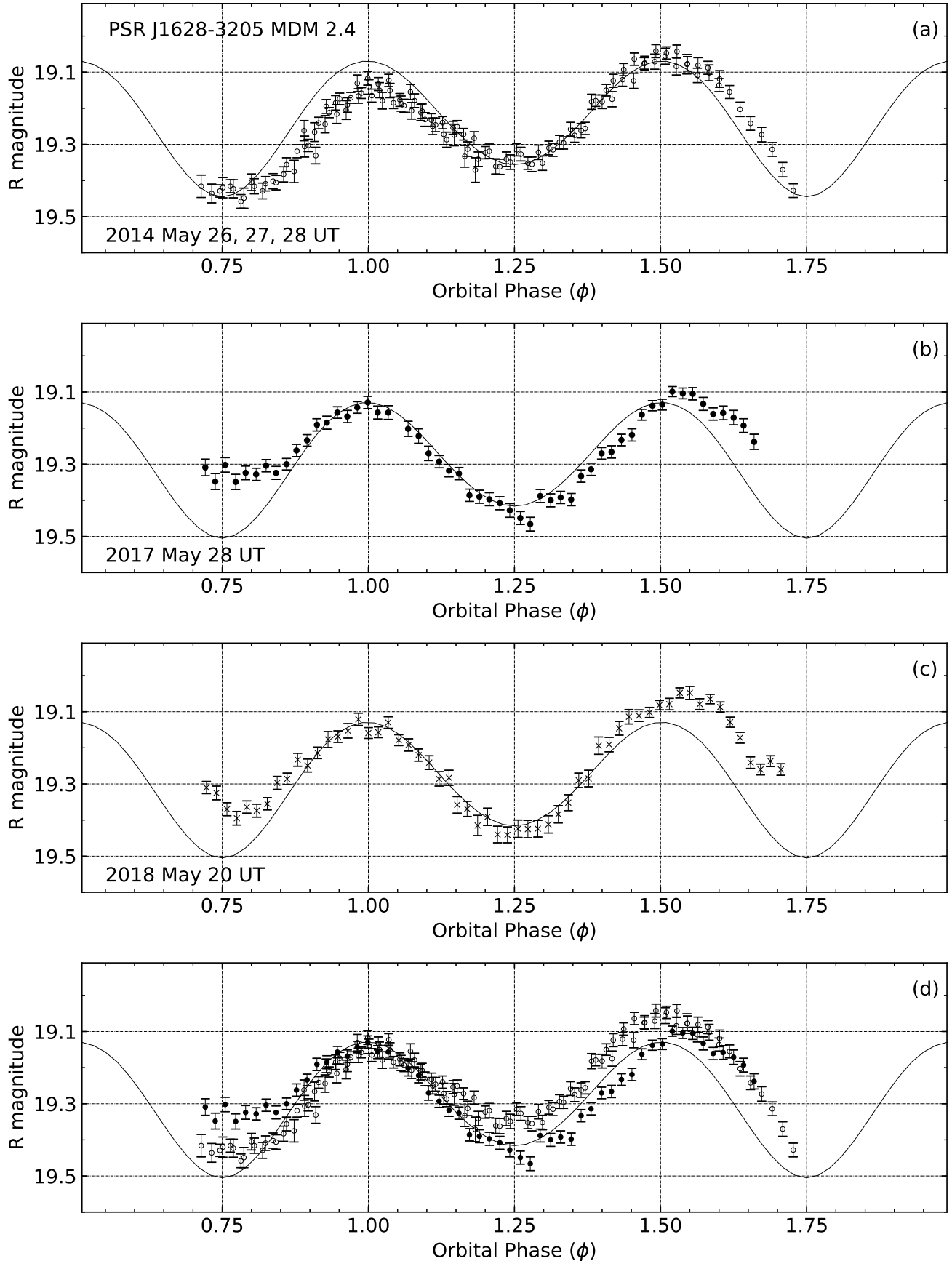


Figure 6. *R*-band light curves of PSR J1628–3205. (a) three consecutive nights in 2014 May superposed, adapted from Li et al. (2014). The curve is an ellipsoidal model from that paper, with inclination angle $i = 75^\circ$. (b) a new *R*-band light curve obtained on 2017 May 28, with the same model curve displaced by 0.06 mag. (c) the latest *R*-band light curve, obtained on 2018 May 20, is very similar to the one from 2017. (d) comparison of 2014 and 2017 data.

curve for PSR J1628–3205 that covered almost a full orbital period (also shown in Figure 6). We observe that the minimum at phase $\phi = 0.25$ has become ≈ 0.1 mag fainter than in 2014, while the minimum at $\phi = 0.75$ has become ≈ 0.1 mag brighter. The maxima at phases $\phi = 0.5$ and $\phi = 0$ are still unequal, and the minimum at $\phi = 0.75$ and the maximum at $\phi = 0.5$ are delayed by about 0.05 in phase. One more observation was made in 2018 May (Figure 6), and the resulting light curve is little changed from 2017 May. Systematic variation from year to year due to the calibration process is limited to ± 0.01 mag, so the observed changes must be real.

Thus, three changes can be discerned between 2014 and 2017. First, the respective heights of the two minima in the light curve are inverted. In 2014, the interpretation of the minima was that pulsar heating is minimal. But in 2017, the higher brightness at $\phi = 0.75$ than at $\phi = 0.25$ suggests that pulsar heating has increased. However, it is difficult to explain why the absolute level at $\phi = 0.25$ decreased in 2017 unless in 2014 there was some pulsar wind being channeled to the “night” side of the companion by its own magnetic field, an effect that is no longer present in 2017. In any case, it seems that variable heating by the pulsar does play a role in this system.

Second, the unheated parts of the companion in 2017 seem to be on average fainter than they were in 2014. Although there is still some asymmetry in the light curve, which was attributed in 2014 to a shock that is skewed toward the trailing side of the companion, that effect is less pronounced in 2017. The decrease in overall flux may suggest a decrease in radius of the companion. The persistence of high-amplitude orbital modulation indicates that the companion star is still tidally distorted, but it may have shrunk slightly.

The third change is that in 2017 the minimum at $\phi = 0.75$, and possibly the one at $\phi = 0.25$, are delayed by about 0.05 in phase, as is the maximum at $\phi = 0.5$, while in 2014 only the minimum at $\phi = 0.75$ was lagging. These changing phase shifts are further evidence of variability due to asymmetric heating from the pulsar or other causes intrinsic to the companion such as the distribution of large star-spots or magnetic activity cycles.

6. DISCUSSION

All three systems studied here are redback MSPs in the non-accreting state, as evidenced by their magnitudes, red colors, and substantial orbital modulation. They have low-mass, nearly Roche-lobe filling companion stars that are tidally distorted and heated by the pulsar wind. The light curves of redbacks can be classified according to whether the modulation is dominated by pulsar wind heating or ellipsoidal geometry. PSR J1048+2339 and XMMU J083850.38–282756.8 are strongly heated, and exhibit significant changes on time scales of weeks to months, which we interpret as structural variations in the heating mechanism. The little data that we have on PSR J1628–3205 also shows variations in the heating pattern between observations obtained in 2014 and 2017, albeit at a lower level compared to its dominant ellipsoidal modulation.

The light curves and variability of PSR J1048+2339 and XMMU J083850.38–282756.8 are very similar to each other. Both have $\approx 0.5 - 1$ mag orbital variation

due to pulsar heating, with the larger-amplitude episodes associated with rapid flaring. Even when flaring is absent, the light curve is asymmetric about the line between stars, usually sloping downward in the phase range $0.5 < \phi < 1.0$. Very similar behavior (Woudt et al. 2004; Thorstensen & Armstrong 2005) is seen from the transitional MSP J1023+0038 in its radio-pulsar state. An asymmetric heating distribution produced by an intrabinary shock distorted by orbital motion could explain part of the modulation (Romani & Sanchez 2016). However, the modeled asymmetries are not great enough to account for the observed discrepancy between the brighter and fainter magnitudes of the slope. Magnetic fields channeling pulsar wind particles and radiation directly onto the surface of the companion have been suggested to account for the remainder of the observed asymmetry (Li et al. 2014; Tang et al. 2014; Sanchez & Romani 2017).

Repeated observations spaced by a few days to a few months allowed us to investigate variable heating in detail. The largest changes in the light curves occur at phase $\phi = 0.75$ for PSR J1048+2339 and XMMU J083850.38–282756.8, where pulsar heating is expected to be most visible. On timescales of weeks or months, the brightness at this phase varies by 0.2 to 0.4 mag, with an additional 0.5 mag increase when in a flaring state. Even in the faintest states of these two pulsars, inferior conjunction of the companion ($\phi = 0.25$) is always fainter than superior conjunction ($\phi = 0.75$), indicating that pulsar heating is always important. From their preferred orbital phases, the optical flares appear to be located on or near the heated face of the companion, although a bright X-ray/optical flare was seen from XMMU J083850.38–282756.8 at the opposite phase (Figure 5). Also, there is the case of PSR J1311–3430, a frequently flaring BW that has flares at all phases (An et al. 2017).

The X-ray flare seen in one of the three *Chandra* observations of PSR J1048+2339 has a peak luminosity of $\approx 10^{33}$ erg s $^{-1}$, which is a significant fraction, $\approx 12\%$ of the pulsar’s spin-down power. The bolometric luminosity of the probable non-thermal spectrum is likely to be even larger, which suggests that some stored energy in magnetic field is being released. The photon spectral index as hard as $\Gamma = 1.2$ in this flare, and in the persistent emission of other redbacks, can be taken as evidence that magnetic reconnection in a striped pulsar wind, rather than shock acceleration, is responsible for energizing synchrotron emitting electrons. See the discussion in Al Noori et al. (2018) of this point, in the context of the persistent X-ray emission of the redback PSR J2129–0429. Since there is no simultaneous optical observation of this event, it is difficult to know if it is associated with an optical flaring episode, via direct emission or reprocessing. However, it seems that X-ray flares are common enough in PSR J1048+2339 and XMMU J083850.38–282756.8 that several could have occurred during our > 30 optical observations of these systems.

In 2.4 years of monitoring PSR J1048+2339, we have seen at least two “cycles” in heating amplitude, although there may have been more events in the interval from 2017 April to December when there were no observations. There is evidently some mechanism that modulates the strength of the pulsar wind heating on a

timescale of months. The duration of the flaring state is difficult to pin down. In retrospect, it lasted at least 3 months (2016 December to 2017 March) in XMMU J083850.38–282756.8, which was the span of observations in Halpern et al. (2017b), but it had stopped when observations resumed 9 months later (2017 November). For PSR J1048+2339 we have only observed flaring during the three (consecutive) nights of this program (2018 April 19–21), whereas there was minimal heating and no flaring 2 months earlier and 1 month later.

PSR J1628–3205 displays the same sort of variable and asymmetric pulsar wind heating, albeit at a lower level compared to the ellipsoidal modulation in this system. The two maxima of the light curves are unequal, and the minimum at $\phi = 0.75$ is often higher than the one at $\phi = 0.25$, both effects indicating a heating contribution. The phase delays of the $\phi = 0.5$ (higher) maximum and the $\phi = 0.75$ minimum indicate that the heating has the same sense of asymmetry that characterize PSR J1048+2339, XMMU J083850.38–282756.8, and PSR J1023+0038. In addition, there is evidence for variable heating even at $\phi = 0.25$ in PSR J1628–3205. This unexpected effect may be due to a process in which magnetic fields intrinsic to the companion channel pulsar wind to localized areas (Sanchez & Romani 2017), including the “night” side of the companion. Possible mechanisms include a magnetic field which shifts in azimuth to channel the pulsar wind to different locations on the companion, or a large, migrating star spot. Strong magnetic fields and large starspots can be expected on rapidly rotating, tidally locked stars. van Staden & Antoniadis (2016) found evidence for differential rotation of such spots during intensive monitoring of the light curve of the redback PSR J1723–2737, which sometimes showed a period slightly different from the orbital period.

Finally, we note that some of the more extreme light curve shapes and variations that we observe may help to understand the optical data on other putative redback MSPs for which a pulsar has not yet been detected and spectroscopic radial velocities are not yet available to establish the orbital phase. In particular, the double-peaked and asymmetric 5.47 hr orbital light curve of the putative counterpart of 3FGL J2039.6–5618 (Romani 2015; Salvetti et al. 2015) resembles closely those of PSR J1628–3205, and especially PSR J1048+2339 during its epochs of weaker heating. Indeed, Salvetti et al. (2015) had to develop a model involving asymmetric heating along the lines discussed here to fit the optical light curve of 3FGL J2039.6–5618. It will be interesting to see, when the absolute phasing of that system is accomplished, if their phase assumptions were correct.

7. CONCLUSIONS

Comparisons among light curves collected over intervals of days to years show clear indications of variable heating in the three redback MSPs observed. The pulsar wind heating is generally off-center, manifested as shifts in the intensity and phase of the extrema of the light curves from expected symmetry based on the radio ephemerides. Generally, the companion star is brighter at $\phi = 0.5$ than at $\phi = 1.0$, which would imply that its trailing side is hotter than its leading side. The light curves exhibit changes on time scales of weeks to months, which may be due to changing magnetic fields intrinsic

to the companion star channeling the pulsar wind to localized areas, or migrating star spots. The largest variations are centered around superior conjunction of the secondary ($\phi = 0.75$), and include episodes of decreased heating as well as flaring.

We suggest that these behaviors may be due to shifts in magnetic fields channeling the pulsar wind or non-synchronous rotation which repeats on time scales of months to years. Given the apparent cyclic nature of the variability, it seems plausible that the mechanism must be at least partly if not wholly due to the latter and may reflect a combination of both. Continued optical observations will more definitively characterize this episodic variability. Further X-ray monitoring of these objects could also examine the geometry and stability of the intrabinary shocks in more detail, and investigate the locations of X-ray flares, whether in the shock or on the companion. Simultaneous X-ray and optical spectroscopy of flares would be especially informative about their origin.

8. ACKNOWLEDGEMENTS

This work is based on observations obtained at the MDM Observatory, operated by Dartmouth College, Columbia University, The Ohio State University, Ohio University, and the University of Michigan. Support for this work was provided by the National Aeronautics and Space Administration through *Chandra* Award Number SAO G07-18047X issued by the *Chandra X-ray Observatory* Center, which is operated by the Smithsonian Astrophysical Observatory for and on behalf of the National Aeronautics and Space Administration under contract NAS8-03060.

REFERENCES

- Alpar, M. A., Cheng, A. F., Ruderman, M. A., & Shaham, J. 1982, *Nature*, 300, 728
- Al Noori, H., Roberts, M. S. E., Torres, R. A., et al. 2018, *ApJ*, 861, 89
- An, H., Romani, R. W., Johnson, T., Kerr, M., & Clark, C. J. 2017, *ApJ*, 850, 100
- Archibald, A. M., Stairs, I. H., Ransom, S. M., et al. 2009, *Science*, 324, 1411
- Bogdanov, S., Archibald, A. M., Hessels, J. W. T., et al. 2011, *ApJ*, 742, 97
- Bogdanov, S., Esposito, P., Crawford, F., et al. 2014a, *ApJ*, 781, 6
- Bogdanov, S., Patruno, A., Archibald, A. M., et al. 2014b, *ApJ*, 789, 40
- Breton, R. P., van Kerkwijk, M. H., Roberts, M. S., E., et al. 2013, *ApJ*, 769, 108
- Cordes, J. M., & Lazio, T. J. W. 2002, arXiv:astro-ph/0207156
- Deneva, J. S., Ray, P. S., Camilo, F., et al. 2016, *ApJ*, 823, 105
- Flewelling, H., Magnier, E., Chambers, K., et al. 2016, arXiv:1612.05243
- Gaia Collaboration, Prusti, T., de Bruijne, J. H. J., et al. 2016a, *A&A*, 595, A1
- Gaia Collaboration, Brown, A. G. A., Vallenari, A., et al. 2016b, *A&A*, 595, A2
- Gentile, P. A., Roberts, M. S. E., McLaughlin, M. A., et al. 2014, *ApJ*, 783, 69
- Halpern, J. P., Bogdanov, S., & Thorstensen, J. R. 2017a, *ApJ*, 838, 124
- Halpern, J. P., Strader, J., & Li, M. 2017b, *ApJ*, 844, 150
- Kalberla, P. M. W., Burton, W. B., Hartmann, D., et al. 2005, *A&A*, 440, 775
- Kong, A. K. H., Huang, R. H. H., Cheng, K. S., et al. 2012, *ApJL*, 747, L3
- Li, K.-L., Hou, K., Strader, J., et al. 2018, *ApJ*, 863, 194
- Li, M., Halpern, J. P., & Thorstensen, J. R. 2014, *ApJ*, 795, 115

- Martini, P., Stoll, R., Derwent, M. A., et al. 2011, *PASP*, 123, 187
- Mirabal, N., Fras-Martinez, V., Hassan, T., & Fras-Martinez, E. 2012, *MNRAS*, 424, L64
- Phinney, E.S., Evans, C.R., Blandford, R.D., & Kulkarni, S.R. 1988, *Nature*, 333, 30
- Roberts, M. S. E. 2013, in *Proc. IAU Symp. 291, Neutron Stars and Pulsars: Challenges and Opportunities after 80 years*, ed. J. van Leeuwen (Cambridge: Cambridge Univ. Press), 127
- Romani, R. W. 2015, *ApJL*, 812, L24
- Romani, R. W., & Shaw, M. S. 2011, *ApJL*, 743, 26
- Romani, R. W., & Sanchez, N. 2016, *ApJ*, 828, 7
- Salvetti, D., Mignani, R. P., De Luca, A., et al. 2015, *ApJ*, 814, 888
- Sanchez, N., & Romani, R. W. 2017, *ApJ*, 845, 42
- Schnitzeler, D. H. F. M. 2012, *MNRAS*, 427, 664
- Schroeder, J., & Halpern, J. 2014, *ApJ*, 793, 78
- Shklovskii, I. S. 1970, *SvA*, 13, 562
- Tang, S., Kaplan, D. L., Phinney, E. S., et al. 2014, *ApJL*, 791, 5
- Thorstensen, J. R., & Armstrong, E. 2005, *ApJ*, 130, 759
- van Staden, A. D., & Antoniadis, J. 2016, *ApJL*, 833, L12
- Wadiasingh, Z., Harding, A. K., Venter, C., Böttcher, M., & Baring, M. G. 2017, *ApJ*, 839, 80
- Woudt, P. A., Warner, B., & Pretorius, M. L. 2004, *MNRAS*, 351, 1015
- Yao, J. M., Manchester, R. N., & Wang, N. 2017, *MNRAS*, 835, 29